Reduced basis method for simulation of nanodevices

George S. H. Pau*
Lawrence Berkeley National Laboratory, 1 Cyclotron Road, MS 50A-1148 Berkeley, California 94720, USA
(Received 27 May 2008; revised manuscript received 12 September 2008; published 24 October 2008)

Ballistic transport simulation in nanodevices, which involves self-consistently solving a coupled Schrödinger-Poisson system of equations, is usually computationally intensive. Here, we propose coupling the reduced basis method with the subband decomposition method to improve the overall efficiency of the simulation. By exploiting *a posteriori* error estimation procedure and greedy sampling algorithm, we are able to design an algorithm where the computational cost is reduced significantly. In addition, the computational cost only grows marginally with the number of grid points in the confined direction.

DOI: 10.1103/PhysRevB.78.155425 PACS number(s): 02.70.−c, 75.40.Mg, 73.23.Ad

I. INTRODUCTION

As size of electronic devices shrinks to nanometer scale, ballistic charge transport becomes increasingly important in describing the transport phenomena in these devices.[1] However, its simulation is usually computationally intensive—we must self-consistently solve a coupled Schrödinger-Poisson system of equations.[2–4] Described in greater detail in Sec. II, the iterative procedure involves repetitively solving a Schrödinger equation with open boundary conditions[2] at many different energy states within each iteration. The large number of states required to accurately determine the distribution of the electron density and the number of self-consistent iterations needed to achieve convergence lead to the large computational cost usually associated with ballistic charge transport simulation. A more efficient method to solve the Schrödinger equation can thus greatly improve the overall efficiency of ballistic charge transport simulation. Note that another popular approach to ballistic transport simulation involves solving the nonequilibrium Green's function equations (NGEF)–Poisson system of equations.[5,6] In this paper, we will concentrate on the approach based on the Schrödinger equation although the methodology we describe can potentially be applied to the NGEF approach as well.

To solve the Schrödinger equation, the finite difference method and the finite element method are the most widely used methods due to their flexibility.[3,4,7–9] However, a direct application of these methods, especially in higher spatial dimensions, can lead to a large algebraic system of equations, of which the solution is computationally expensive. The subband decomposition method[10,11] or more commonly known as the coupled-mode approach[5,12] attempts to reduce the computational cost by decomposing the Schrödinger equation into two smaller subproblems, resulting in a bounded Schrödinger equation in the confined directions and an open Schrödinger equation in the transport direction. In particular, by first solving the bounded Schrödinger equation at different locations along the transport direction, we are able to obtain a smaller algebraic system of equations for the open Schrödinger equation, which can then be solved more efficiently; the procedure is then effective in the limit where we need to solve the Schrödinger equation at large number of different energy levels. The efficiency can be further improved by a WKB approximation of the open Schrödinger equation.[11] Nevertheless, solving the bounded Schrödinger equation, which involves solving an eigenvalue problem at different locations along the transport direction, can still be potentially expensive, especially when strong confinement of the electron demands a finely discretized simulation domain. This paper proposes an efficient method based on the reduced basis approach to reduce the computational cost of solving the bounded Schrödinger equation.

The reduced basis method is a model-order reduction technique which exploits dimension reduction afforded by the *smooth* and *low-dimensional* parametrically induced solution manifold. Instead of using general basis sets such as finite element, an approximation to a solution of an underlying parametrized partial differential equation (PDE) is obtained by a projection onto a finite and low-dimensional vector space spanned by a basis set consisting of solutions at a number of judiciously selected parameter points. The reduced basis method was first introduced in the late 1970s in the context of nonlinear structural analysis[13,14] and subsequently abstracted, analyzed, and extended to a much larger class of parametrized partial differential equations.[15–19] In the more recent past the reduced basis approach and in particular associated *a posteriori* error estimation procedures have been successfully developed for many different types of PDEs that are affine in the parameters,[20–26] general nonaffine PDEs,[27,28] and linear eigenvalue problem.[21,29] We will elaborate further the methodology in Sec. III. In particular, we extend the methodology described in Ref. 29 to eigenvalue problem that is nonaffine in the parameter, and describe how reduced basis methodology can be incorporated into the overall solution procedure for the Schrödinger-Poisson system of equations.

This paper is organized as follows. We first describe the problem that we would like to solve. To simplify the presentation of the methodology, we will use the double-gate metal-oxide-semiconductor field-effect transistor (MOSFET) as a model problem (Fig. 1). We then provide the weak formulation of the equations involved and briefly describe the subband decomposition method. This serves as a platform for us to describe the reduced basis method, and how it fits into the overall solution procedure. We conclude with some numerical results and comparison to the subband decomposition method. This paper utilizes atomic units for all quantities; conversions between atomic units and some common units for quantities relevant to this paper are listed in Appendix A.

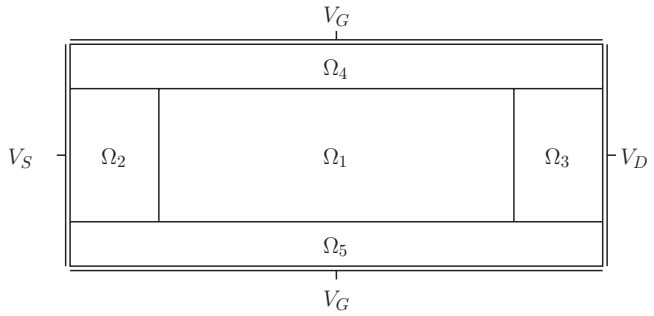

FIG. 1. A model problem based on the double-gate MOSFET.

II. PROBLEM STATEMENT

With the effective-mass approximation,[30] the electron is described by a wave function $\psi(E) \in H^1(\Omega) \subset \mathbb{C}^2$ which for a given E, satisfies the following Schrödinger equation:

$$-\nabla \cdot \left(\frac{1}{2m^*} \nabla \psi(E) \right) + V_{\text{eff}}(\psi)\psi(E) - E\psi(E) = 0, \quad (1)$$

with appropriate open boundary conditions.[2] The potential $V_{\text{eff}} \in L^2(\Omega)$ is given by

$$V_{\text{eff}}(\psi) = -\phi(\psi) + V_{xc}(\psi) + V_b, \quad (2)$$

where $\phi \in H^1(\Omega)$, $V_{xc} \in H^1(\Omega)$ and $V_b \in L^2(\Omega)$. We ignore the exchange-correlation term V_{xc} for simplicity but the methodology described will easily accommodate the V_{xc} term, and V_b describes the potential gap between the insulator and the semiconductor. The potential ϕ in turn satisfies a Poisson equation given by

$$-\nabla \cdot [\epsilon \nabla \phi] = -n(\psi) + N_D, \quad (3)$$

with appropriate boundary conditions. Here, ϵ is the dielectric function of the materials, $n(\psi)$ is the density of free electrons, and N_D is the concentration of donor impurities; we ignore contribution of hole and acceptor impurities for simplicity. Equations (1) and (2) are thus coupled through the term $n(\psi)$, which can be defined as

$$n(\psi) = \int_{-\infty}^{\infty} g(E(\mathbf{k}))|\psi(E(\mathbf{k}))|^2 d\mathbf{k}, \quad (4)$$

where g is the statistics of the electrons injected into the device with energy $E(\mathbf{k})$, $\mathbf{k}$ is the wave vector, and E is a function of $\mathbf{k}$. A more complete definition, specific to the model problem we intend to solve, is given by Eq. (17).

To solve the above coupled system of equations, we will use a fixed-point method. Starting from an initial guess n^0, we construct the sequence n^k where n^k is determined from Eq. (4) with ψ^k computed from Eq. (1) with $V_{\text{eff}} = \phi^k + V_b$. We note that Eq. (4) must be evaluated numerically, and thus Eq. (1) must be evaluated many times. We then solve Eq. (3) for ϕ^{k+1} with the new value of n^k. The procedure is repeated until $\|\phi^k - \phi^{k-1}\|_{L_2} / \|\phi^k\|_{L_2} \leq \varepsilon_{\text{tol}}$, where ε_{tol} is our desired tolerance and $\|\cdot\|_{L_2}$ is the L_2 norm. To improve the convergence rate of the algorithm, we follow the suggestion in Ref. 6—we substitute Eq. (3) with the following nonlinear Poisson equation:

$$-\nabla \cdot [\epsilon \nabla \phi^{k+1}] + n_{3\text{D}} f_{1/2}\left(\frac{\phi^{k+1} - F_n^k}{T} \right) = N_D, \quad (5)$$

where $n_{3\text{D}}$ is the three-dimensional effective density of states, f_α is the Fermi-Dirac integral of order α, and F_n^k is the quasi-Fermi level defined as

$$F_n^k = \phi^k - T f_{1/2}^{-1}\left(\frac{n^k}{n_{3\text{D}}} \right). \quad (6)$$

For the purpose of this paper, we will consider a two-dimensional nanodevice (a double-gate MOSFET) shown in Fig. 1. Given a source potential V_S, a drain potential V_D, and a gate potential V_G, we would like to determine the current flow I in the x_1 direction. The simulation domain $\Omega \equiv [0,a] \times [0,b] \subset \mathbb{R}^2$ can be further divided into five subdomains denoted by Ω_i, $i=1,\ldots,5$; (x_1,x_2) denotes a point in Ω. The material properties we will be using is that of Si in Ω_1, Ω_2 and Ω_3, and SiO_2 in Ω_4 and Ω_5. In addition, Ω_2 and Ω_3 are doped to provide free carriers for the charge transport. We assume the crystal structure of the device is oriented such that x_1 is in the $\langle 100 \rangle$ direction and x_2 is in the $\langle 001 \rangle$ direction. The axes are then aligned with the principal axes of the six equivalent ellipsoids of the conduction band. Based on the effective-mass approximation, we then have three configurations for $m^* \equiv (m_1^*, m_2^*, m_3^*)$ and

$$\nabla \cdot \left(\frac{1}{2m^*} \nabla \psi \right) = \frac{\partial}{\partial x_1}\left(\frac{1}{2m_1^*} \frac{\partial}{\partial x_1} \psi \right) + \frac{\partial}{\partial x_2}\left(\frac{1}{2m_2^*} \frac{\partial}{\partial x_2} \psi \right) + \frac{\partial}{\partial x_3}\left(\frac{1}{2m_3^*} \frac{\partial}{\partial x_3} \psi \right).$$

The three configurations of m^* are given by (m_l, m_t, m_t), (m_t, m_l, m_t), and (m_t, m_t, m_l); m_t and m_l are the transverse and longitudinal masses of the material. We assume m_t and m_l for Si and SiO_2 are the same. Finally, we assume we have a two-dimensional electron gas with a parabolic dispersion relation in the x_3 direction.

A. Abstract formulation

We now derive the weak formulation for Eqs. (1) and (3) for the model problem described in Sec. II. For Eq. (1), the weak formulation is as follows: given $E \in \mathbb{R}$, find $\psi \in Y \equiv H^1(\Omega)$ such that

$$\frac{1}{2m_1^*} \int_\Omega \frac{\partial \psi}{\partial x_1} \frac{\partial v^*}{\partial x_1} + \frac{1}{2m_2^*} \int_\Omega \frac{\partial \psi}{\partial x_2} \frac{\partial v^*}{\partial x_2} + \int_\Omega \psi V_{\text{eff}} v^* - E \int_\Omega \psi v^* = \frac{1}{2m_1^*} \int_{\Gamma_S \cup \Gamma_D} \frac{\partial \psi}{\partial x_1} v^*, \quad \forall v \in Y, \quad (7)$$

where Γ_S and Γ_D are, respectively, the boundaries in contact with source and drain electrodes. Based on the quantum transmitting boundary method,[2] we expand the right-hand side of Eq. (7): for $g = S, D$,

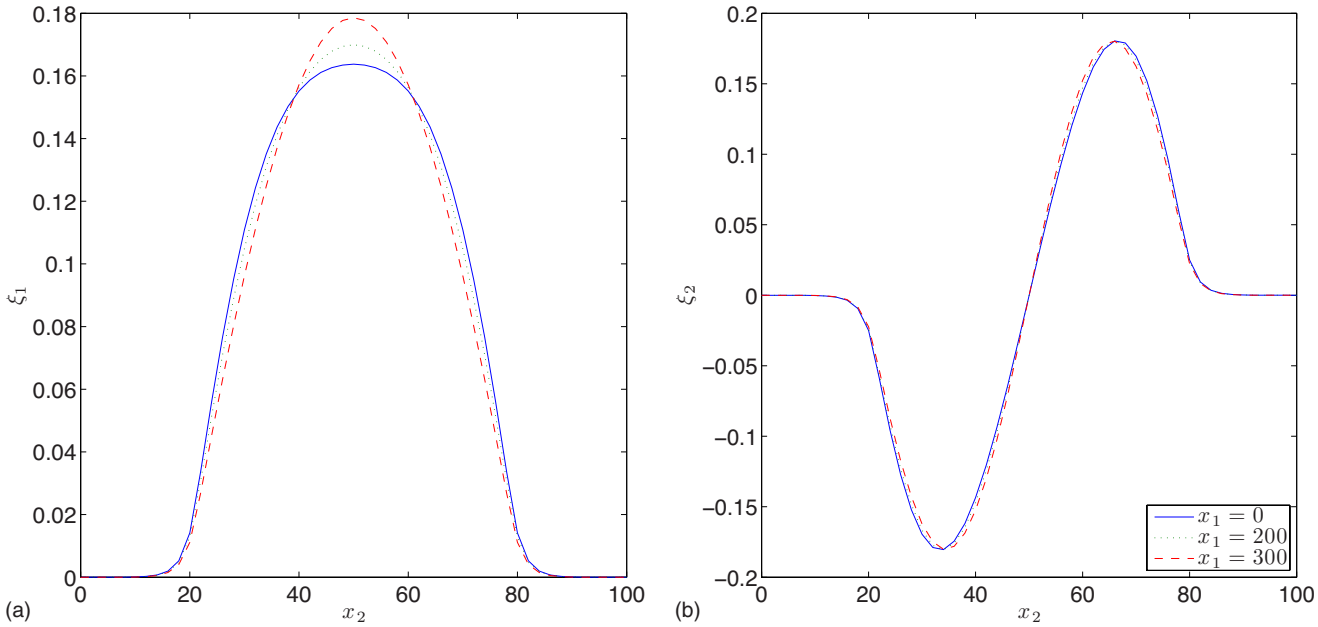

FIG. 2. (Color online) ξ_1 and ξ_2 for three different values of x_1 based on FE approximation for V_D=0.015.

$$\int_{\Gamma_g} \frac{\partial \psi}{\partial x_1} v^* = -\sum_{m=1}^{N^g} i2a_m^g k_m^g \int_{\Gamma_g} \chi_m^g v^* + \sum_{m=1}^{N^g} ik_m^g \int_{\Gamma_g} \chi_m^g v^* \int_{\Gamma_g} \chi_m^g \psi - \sum_{m=N^g+1}^{\infty} k_m^g \int_{\Gamma_g} \chi_m^g v^* \int_{\Gamma_g} \chi_m^g \psi, \tag{8}$$

where (ξ_m^g, E_m^g), $1 \le m \le \infty$ are the eigenstates along Γ_g; $k_m^g = \sqrt{2m^*|E - E_m^g|}$; N^g is the largest m for which $E > E_m^g$, b_m^g, $1 \le m \le N^g$ are the coefficients of outgoing traveling-wave states, and b_m^g, $m > N^g$ are coefficients of the evanescent states. For a particular problem, a_m^g is a parameter that we can vary while b_m^g and N^g are determined as part of the solution.

To facilitate the variational formulation, we now define the following functional forms: $\forall w \in Y$, $v \in Y$, $V \in L^2$, $\chi^g \in H_0^1(\mathbb{R})$,

$$a_0(w,v;\alpha) = \int_\Omega \alpha \nabla w \nabla v^*, \tag{9}$$

$$a_1(w,v;m^*) = \frac{1}{2m_1^*} \int_\Omega \frac{\partial w}{\partial x_1} \frac{\partial v^*}{\partial x_1} + \frac{1}{2m_2^*} \int_\Omega \frac{\partial w}{\partial x_2} \frac{\partial v^*}{\partial x_2}, \tag{10}$$

$$a_2(w,v;V) = \int_\Omega wVv^*, \tag{11}$$

$$a_3(w,v) = \int_\Omega wv^*, \tag{12}$$

$$c(w,v;\chi^g) = \frac{1}{2m_1^*} \int_{\Gamma_g} \chi^g w \int_{\Gamma_g} \chi^g v^*, \tag{13}$$

$$b(v;\chi^g) = \frac{1}{2m_1^*} \int_{\Gamma_g} \chi^g v^*. \tag{14}$$

The abstract formulation is then as follows: given $E \in \mathbb{R}$, find $\psi \in Y$ that satisfies

$$a_1(\psi,v;m^*) + a_2(\psi,v;V_{\text{eff}}) - Ea_3(\psi,v) - \sum_{g=S,D} \sum_{m=1}^{N^g} ik_m^g c(\psi,v;\chi_m^g) + \sum_{g=S,D} \sum_{m=N^g+1}^{\infty} k_m^g c(\psi,v;\chi_m^g) = -\sum_{g=S,D} \sum_{m=1}^{N^g} i2a_m^g k_m^g b(v;\chi_m^g), \quad \forall v \in Y. \tag{15}$$

For Eq. (5), the weak formulation is as follows: given $n(\psi)$ the solution $\phi \in H^1(\Omega)$ is given by

$$\int_{\Omega/\Gamma_0} \epsilon \nabla \phi \nabla v^* + \int_{\Gamma_0} \epsilon \nabla V_G \nabla v^* + \int_\Omega n_\phi(\phi, n(\psi)) v^* = \int_\Omega N_D v^*, \quad \forall v \in Y,$$

where Γ_0 is the boundary in contact with gate electrode, and $n_\phi(\phi, n(\psi)) = n_{3D} f_{1/2}(\frac{\phi - F_n(n(\psi))}{T})$. We have imposed the following boundary conditions:

$$\phi|_{\Gamma_0} = 0, \quad \text{and} \quad \left.\frac{d\phi}{dx_1}\right|_{\Gamma_S \cup \Gamma_D} = 0.$$

Let $f(v;V) = \int_\Omega Vv^*$, and $h(v;V) = \int_{\Gamma_0} \epsilon \nabla V \nabla v^*$. Then, the abstract formulation is as follows: given $n(\psi)$, the solution $\phi \in Y$ is given by

$$a_0(\phi,v;\epsilon) + f(v;n_\phi(\phi,n(\psi))) = f(v;N_D) - h(v;V_G), \tag{16}$$

$$\forall v \in Y.$$

For the current problem where we have assumed a two-dimensional electron gas, the charge density n is given by[6]

$$n(\psi) = \sum_{g=S,D} \sum_{m=1}^{N^g} \sqrt{\frac{m_3^* T}{2\pi^3}} \int_0^\infty f_{-1/2}\left(\frac{E_{f,g} - E(\mathbf{k})}{T}\right) \times |\psi(E(\mathbf{k}), a_m^g)|^2 d\mathbf{k}, \tag{17}$$

and this is summed over the three different configurations of m^*. In Eq. (17), $E_{f,S}$ and $E_{f,D}$ are the Fermi levels at the source and drain, which we assume to be zero at zero bias. In addition, we assume quadratic band structure where $E(\mathbf{k}) = E_{\min} + \frac{|\mathbf{k}|^2}{2m^*}$ and $E_{\min}$ is the lowest energy occupied by the electrons. Finally, the current intensity I is given by

$$I = \int_0^b j_1(x_1, x_2; \psi) dx_2, \tag{18}$$

where j_1, the current density in the x_1 direction, is defined as

$$j_1(\psi) = \sum_{g=S,D} \sum_{m=1}^{N^g} \frac{1}{m_1^*} \sqrt{\frac{m_3^* T}{2\pi^3}} \times \int_0^\infty \mathrm{Im}\left\{\bar{\psi}(E(\mathbf{k}), a_m^g) \frac{\partial \psi(E(\mathbf{k}), a_m^g)}{\partial x_1}\right\} \times f_{-1/2}\left(\frac{E_{f,g} - E(\mathbf{k})}{T}\right) d\mathbf{k}. \tag{19}$$

Numerical approximation of Eqs. (15) and (16) based on, say, finite element method, can however be computationally very expensive since Eq. (15) must be solved many times in a single iteration in order to numerically determine the density n. In particular, suppose we substitute the unbounded upper limit in Eq. (17) by $\mathbf{k}_{\max} = \sqrt{2m_1^* E_{\max}}$ and subdivide the interval $[0, \mathbf{k}_{\max}]$ into $n_\mathbf{k}$ intervals. We then use Gauss quadrature formulation within each interval to arrive at the following approximation of n:

$$n(\psi) \approx \sqrt{\frac{m_3^* T}{2\pi^3}} \sum_{g=S,D} \sum_{m=1}^{N^g} \sum_{i=1}^{n_\mathbf{k}} \sum_{q=1}^{Q} f_{-1/2}\left(\frac{E_{f,g} - E(\mathbf{k}_q^i)}{T}\right) \times |\psi(E(\mathbf{k}_q^i); a_m^g)|^2 w_q, \tag{20}$$

where N^g is the number of modes considered at Γ_g; $a_{m'}^{g'} = 1$ if $m' = m$ and $g' = g$, and 0 otherwise; $\mathbf{k}_q^i$ are the quadrature points in interval i; w_q is the quadrature weight; and Q is the number of quadrature points used per interval. Then, in each iteration, the maximum number of times we must solve Eq. (15) is $(N^S + N^D) n_\mathbf{k} Q$. This can be somewhat smaller by excluding E for which $f_{-1/2}([E_{f,g} - E(\mathbf{k})]/T)$ is negligibly small.

B. Subband decomposition approach

The subband decomposition method is first described in Refs. 5 and 10. Assuming that the wave function is bounded in the x_2 direction, we can write Y as $X^1 \times X^2$ where $X^1 = H^1(\Omega^1 \equiv [0,a])$ and $X^2 = H_0^1(\Omega^2 \equiv [0,b])$. Then, we can express $\psi \in Y$ as

$$\psi(x;E) = \sum_{i=1}^{\infty} \varphi_i(x_1;E)\xi_i(x_2;x_1), \quad \varphi_i(x_1;E) \in X^1, \tag{21}$$

$$\xi_i(x_2;x_1) \in X^2.$$

Here, $\xi_i(\cdot;\mu \equiv x_1) \in X^2$, $i = 1, \ldots, \infty$ are solutions to the following eigenvalue problem:

$$\tilde{a}_1(\xi_i(\mu), v; m_2^*) + \tilde{a}_2(\xi_i(\mu), v; V_{\text{eff}}(\mu)) = \lambda_i(\mu)\tilde{a}_3(\xi_i(\mu), v), \quad 1 \le i \le \infty, \quad \forall v \in X^2, \tag{22}$$

$$\tilde{a}_3(\xi_i(\mu), \xi_j(\mu)) = \delta_{ij}, \quad 1 \le i,j \le \infty, \tag{23}$$

where $V_{\text{eff}}(\mu) = V_{\text{eff}}(x_2; \mu \equiv x_1)$, and

$$\tilde{a}_1(w,v;\alpha) = \int_{\Omega^2} \frac{1}{2\alpha} \nabla w \nabla v, \quad \tilde{a}_2(w,v;t) = \int_{\Omega^2} wtv, \quad \tilde{a}_3(w,v) = \int_{\Omega^2} wv, \tag{24}$$

for $w \in X^2$, $v \in X^2$ and $t \in L^2(\Omega^2)$.

Substituting Eq. (21) into Eq. (15), we obtain a one-dimensional problem for $\varphi_i(E)$:

$$\sum_{i=1}^{\infty} \frac{1}{2m_1^*} \left\{ \int_{\Omega^1} \frac{d\varphi_i(E)}{dx_1} \frac{dt}{dx_1} \tilde{a}_3(\xi_i(x_1), \xi_j(x_1)) + \int_{\Omega^1} \frac{d\varphi_i(E)}{dx_1} t(x_1) \tilde{a}_3\left(\xi_i(x_1), \frac{\partial \xi_j}{\partial x_1}(x_1)\right) + \int_{\Omega^1} \varphi_i(x_1;E) \frac{dt(x_1)}{dx_1} \tilde{a}_3\left(\frac{\partial \xi_i}{\partial x_1}(x_1), \xi_j(x_1)\right) + \int_{\Omega^1} \varphi_i(x_1;E) t(x_1) \tilde{a}_3\left(\frac{\partial \xi_i}{\partial x_1}(x_1), \frac{\partial \xi_j}{\partial x_1}(x_1)\right) \right\} + \int_{\Omega^1} [\lambda_i(x_1) - E] \varphi_i(x_1;E) t(x_1) \delta_{ij} - \sum_{g=S,D} \sum_{m=1}^{N^g} i k_m^g \frac{\varphi_i(x_g) t(x_g)}{2m_1^*} \delta_{mi} \delta_{mj} + \sum_{g=S,D} \sum_{m=N^g+1}^{\infty} k_m^g \frac{\varphi_i(x_g) t(x_g)}{2m_1^*} \delta_{mi} \delta_{mj} = - \sum_{g=S,D} \sum_{m=1}^{N^g} i 2 a_m^g k_m^g \frac{t(x_g)}{2m_1^*} \delta_{mj}, \quad \forall t \in X^1, \quad 1 \le j \le \infty. \tag{25}$$

This is simply the weak form for the following one-dimensional Schrödinger equation:[10]

$$-\frac{d}{dx_1}\left(\frac{1}{2m_1^*}\frac{d}{dx_1}\varphi_i\right)-\sum_{j=1}^{\infty}\frac{a_{ij}(x_1)}{m_1^*}\frac{d}{dx_1}\varphi_j - \sum_{j=1}^{\infty}\left(\frac{b_{ij}(x_1)}{2m_1^*}-\lambda_i\delta_{ij}+E\delta_{ij}\right)\varphi_j=0, \tag{26}$$

for $i=1,\ldots,\infty$ with the appropriate open boundary condition; $a_{ij}(x_1)=\int_{\Omega_2}\xi_i(x_1)\{\partial\xi_j(x_1)/\partial x_1\}$ and $b_{ij}(x_1)=\int_{\Omega_2}\xi_i(x_1)\{\partial^2\xi_j(x_1)/\partial x_1^2\}$. It is further found that only finite number of ξ_i is needed, which we denote as n_e. If these n_e $\xi_i(x_1)$ are known, this one-dimensional problem can be solved very efficiently.

In solving Eq. (25), we need to determine $\partial\xi_i/\partial\mu$ as well. Let $\partial\xi_i/\partial\mu\in X^2$. Then, by taking the derivative of Eqs. (22) and (23) with respect to μ, we obtain

$$\tilde{a}_1\left(\frac{\partial\xi_i}{\partial\mu}(\cdot;\mu),v;m_2^*\right)+\tilde{a}_2\left(\frac{\partial\xi_i}{\partial\mu}(\cdot;\mu),v;V_{\text{eff}}(\cdot;\mu)\right) - \lambda_i(\mu)\tilde{a}_3\left(\frac{\partial\xi_i}{\partial\mu}(\cdot;\mu),v\right) = -\tilde{a}_2\left(\xi_i(\cdot;\mu),v;\frac{\partial V_{\text{eff}}(\cdot;\mu)}{\partial\mu}\right)+\frac{d\lambda_i(\mu)}{d\mu}\tilde{a}_3(\xi_i(\cdot;\mu),v),$$

$$1\le i\le\infty,\quad \forall\, v\in X^2, \tag{27}$$

$$\tilde{a}_3\left(\frac{\partial\xi_i}{\partial\mu}(\cdot;\mu),\xi_i(\cdot;\mu)\right)=0. \tag{28}$$

In addition, by letting $v=\xi_i$ and invoking Eq. (22), we have

$$\tilde{a}_1\left(\frac{\partial\xi_i}{\partial\mu}(\cdot;\mu),\xi_i;m_2^*\right)+\tilde{a}_2\left(\frac{\partial\xi_i}{\partial\mu}(\cdot;\mu),\xi_i;V_{\text{eff}}(\cdot;\mu)\right) - \lambda_i(\mu)\tilde{a}_3\left(\frac{\partial\xi_i}{\partial\mu}(\cdot;\mu),\xi_i\right)=0,\quad 1\le i\le\infty, \tag{29}$$

since $\tilde{a}_1$, $\tilde{a}_2$ and $\tilde{a}_3$ are symmetric functionals, and $\partial\xi_i/\partial\mu\in X^2$. Thus, by substituting $v=\xi_i$ into Eq. (27), we obtain

$$\frac{d\lambda_i(\mu)}{d\mu}=\tilde{a}_2\left(\xi_i(\cdot;\mu),\xi_i(\cdot;\mu);\frac{\partial V_{\text{eff}}(\cdot;\mu)}{\partial\mu}\right), \tag{30}$$

since $\tilde{a}_3(\xi_i,\xi_i)=1$. Finally, by substituting Eq. (30) into Eq. (27), we can solve for $\partial\xi_i/\partial\mu$. At present $\partial V_{\text{eff}}/\partial\mu$ is computed using a difference formula. In Appendix C, we describe a formulation that is more consistent with the finite element approximation space of ϕ; it however leads to a higher computational cost. We also note that since V_b does not depend on x_1, $\partial V_{\text{eff}}/\partial\mu=-\partial\phi/\partial\mu$.

The subband decomposition method can now be described as follows. Each fixed-point iteration described in Sec. II involves the following three parts: (i) the determination of the subbands $\xi_i(x_2;x_1)$, $1\le i\le n_e$ for finite points in Ω^1, (ii) the determination of $n(\psi)$ by solving Eq. (25) for $(N^S+N^D)n_EQ$ different combination of E and a_m^g, and (iii) the determination of $\phi(\psi)$ by solving Eq. (16) given $n(\psi)$. In Ref. 10 finite element method is used to approximate the solutions at all stages of the algorithm. It is hoped that the computational overhead incurred in part (i) will significantly reduce the computational cost of solving the open Schrödinger equation needed to determine the electron density. However, part (i) can be computationally expensive, especially if very fine mesh is needed to resolve the strong confinement of the electrons in the x_2 direction or when Eq. (22) must be solved at large number of points if finer mesh is needed in the x_1 direction. Our goal is to speed up the determination of ξ_i for any given x_1 through the reduced basis method.

III. REDUCED BASIS METHOD

Consider a case where $n_e=1$. Let $\mu\equiv x_1$ and $\mathcal{D}\equiv\Omega^1$. Then, a finite element approximation of Eq. (22) entails representing $\xi_1(\mu)$ by a linear combination of the finite element basis functions in a finite element approximation space, $X^{2,\mathcal{N}}\subset X^2$, of dimension $\mathcal{N}-\xi_1(\mu)$ is an arbitrary member of $X^{2,\mathcal{N}}$. However, $\xi_1(\mu)$ can be localized to a much lower lower-dimensional manifold $\mathcal{M}=\{\xi_1(\mu),\mu\in X^1\}$ residing in X^2. This manifold $\mathcal{M}$ can be visualized as a one-dimensional filament that winds through X^2. Presuming that $\mathcal{M}$ is sufficiently smooth, we can then represent $\xi_1(\mu)$ by elements in span $\{\mathcal{M}\}$. This smoothness behavior is evident in Fig. 2 for ξ_1 and ξ_2. The reduced basis method will explicitly exploit this computational opportunity.

This section is organized as follows. We first define the reduced basis approximation spaces that we use to approximate $\xi_i(\mu)$, $1\le i\le n_e$. This is followed by a detailed description of the offline-online computational decomposition strategy—the procedure by which we obtain our computational speedup. We then describe the *a posteriori* error estimation procedure; this allows us to determine the approximate accuracy of the reduced basis approximation to $\xi_i(\mu)$ with marginal additional computational cost. This error estimation procedure will also be used in the construction of the approximation spaces based on the adaptive greedy sampling procedure described next. We conclude this section with a summary of the steps involved in an implementation of the reduced basis method and a description on how reduced basis method can be efficiently integrated within the subband decomposition method. For notational convenience, we have $\xi_i(\mu)=\xi_i(x_2;\mu)$, $\phi(\mu)=\phi(x_2;\mu)$, $d\xi_i(\mu)=\partial\xi_i(x_2;\mu)/\partial\mu$ and $d\phi(\mu)=\partial\phi(x_2;\mu)/\partial\mu$.

A. Approximation spaces

We first introduce nested sample sets $S_N=(\mu_1,\ldots,\mu_{N_s})$, $1\le N_s\le N_{s,\max}$ and define the associated nested reduced basis spaces as

$$W_N=\text{span}\{\xi_i(\mu_j),1\le i\le n_e,1\le j\le N_s\},\quad 1\le N_s\le N_{s,\max},$$

$$=\text{span}\{\zeta_n,1\le n\le N\equiv N_sn_e\},\quad 1\le N_s\le N_{s,\max}, \tag{31}$$

where $\xi_1(\mu_j),\ldots,\xi_{n_e}(\mu_j)$ are the solutions of Eq. (22) at $\mu=\mu_j$, and ζ_n are basis functions obtained after $\xi_i(\mu_j)$, $1\le i\le n_e$, and $1\le j\le N_s$ are orthonormalized. These reduced ba-

sis spaces are constructed based on an adaptive greedy algorithm[23,26] which will be described in Sec. III E, after several components of the algorithm have first been explained in the preceding sections.

We also construct collateral approximation spaces for $\phi(\mu)$ and $d\phi(\mu)$ based on the empirical interpolation procedure.[27,28,31] For $p=\phi(\mu)$ and $d\phi(\mu)$, we construct nested sample sets $S_M^p \equiv \{\mu_1^p, \ldots, \mu_M^p\}$, $1 \le M \le M_{\max}^p$, nested approximation spaces $W_M^p \equiv \text{span}\{q_1^p, \ldots, q_M^p\}$, $1 \le M \le M_{\max}^p$, and nested interpolation points $T_M^p \equiv \{t_1^p, \ldots, t_M^p\}$, $1 \le M \le M_{\max}^p$.

In Eq. (31), we have assumed $\xi_i(\mu_j)$ are known exactly. In practice, however, $\xi_i(\mu_j)$ must be determined through some form of "truth" approximation—here, we use the finite element method with $\mathbb{P}_1$ elements. We build our reduced basis approximation on and measure the error in the reduced basis approximation relative to this truth approximation. Note that since reduced basis approximation is built upon this truth approximation, it cannot perform better than this truth approximation. Thus, the number of elements used to obtain our truth approximation, $\mathcal{N}$, must usually be large. Similarly, the W_M^ϕ and $W_M^{d\phi}$ are constructed from a truth approximation of ϕ and $d\phi$, here based on finite element method utilizing $\mathbb{Q}_2$ elements.

B. Approximation

Our reduced basis approximation to Eqs. (22) and (23) is then given by the following: find $(\xi_{i,N,M}(\mu), \lambda_{i,N,M}(\mu)) \in \mathcal{Y}_N \equiv (W_N \times \mathbb{R})$, $1 \le i \le n_e$ such that

$$\tilde{a}_1(\xi_{i,N,M}(\mu), v; m_2^*) + \tilde{a}_2(\xi_{i,N,M}(\mu), v; V_{\text{eff},M}(\mu)) = \lambda_{i,N,M}(\mu)\tilde{a}_3(\xi_{i,N,M}(\mu), v), \quad 1 \le i \le n_e, \quad \forall\, v \in W_N, \tag{32}$$

$$\tilde{a}_3(\xi_{i,N,M}(\mu), \xi_{j,N,M}(\mu)) = \delta_{ij}, \quad 1 \le i,j \le n_e, \tag{33}$$

where $V_{\text{eff},M} = V_b + \phi_M$.

Similarly, our reduced basis approximation to Eqs. (27) and (28) is given by the following: find $d\xi_{i,N,M}(\mu) \in W_N$, $1 \le i \le n_e$ such that

$$\tilde{a}_1(d\xi_{i,N,M}(\mu), v; m_2^*) + \tilde{a}_2(d\xi_{i,N,M}(\mu), v; V_{\text{eff},M}(\cdot;\mu)) - \lambda_{i,N,M}(\mu)\tilde{a}_3(d\xi_{i,N,M}(\mu), v) = \tilde{a}_2(\xi_{i,N,M}(\mu), v; d\phi_M(\mu)) + \frac{d\lambda_{i,N,M}(\mu)}{d\mu}\tilde{a}_3(\xi_{i,N,M}(\mu), v), \quad 1 \le i \le n_e, \quad \forall\, v \in W_N, \tag{34}$$

$$\tilde{a}_3(d\xi_{i,N,M}(\mu), \xi_{i,N,M}(\mu)) = 0, \tag{35}$$

where

$$\frac{d\lambda_{i,N,M}(\mu)}{d\mu} = \tilde{a}_2(\xi_{i,N,M}(\mu), \xi_{i,N,M}(\mu); d\phi_M(\mu)). \tag{36}$$

It is not immediately clear that $d\xi_{i,N,M}(\mu)$ can be sufficiently approximated in W_N. In Sec. IV, we will examine if it is necessary to replace W_N by an enlarged space W_N^d given by

$$W_N^d = \text{span}\{\xi_i(\mu_j), \ldots, \xi_{n_e}(\mu_j), d\xi_i(\mu_j), \ldots, d\xi_{n_e}(\mu_j), 1 \le j \le N_s\}, = \text{span}\{\zeta_n, 1 \le n \le N \equiv 2N_s n_e\}. \tag{37}$$

C. Offline-online decomposition

We first expand our reduced basis approximation as

$$\xi_{n,N,M}(\mu) = \sum_{j=1}^{N} \xi_{n,N,Mj}(\mu)\zeta_j, \quad 1 \le n \le n_e, \tag{38}$$

where $\zeta_j \in W_N$, and $\xi_{n,N,Mj}(\mu) \in \mathbb{R}$. We then expand our empirical interpolation approximation for $\phi(\cdot;\mu)$ as

$$\phi_M(\cdot;\mu) = \sum_{m=1}^{M^\phi} \beta_{M,m}(\mu) q_m^\phi(\cdot), \tag{39}$$

where $\beta_M(\mu) \in \mathbb{R}^M$ is given by

$$\sum_{k=1}^{M^\phi} B_{m,k}^{M,\phi}\beta_{Mk}(\mu) = \phi(t_m^\phi;\mu), \quad 1 \le m \le M^\phi, \tag{40}$$

and $B^{M,\phi} \in \mathbb{R}^{M^\phi} \times \mathbb{R}^{M^\phi}$ is given by $B_{m,k}^{M,\phi} = q_m^\phi(t_k^\phi)$, $1 \le m,k \le M^\phi$. We note that $\{q_m^\phi, 1 \le m \le M^\phi\}$ is preconstructed based on the empirical interpolation method. Inserting the above representations Eqs. (38) and (39) into Eqs. (32) and (33), we obtain the following discrete equations:

$$\sum_{j=1}^{N} \left\{ A_{i,j}^N + \left(\sum_{m=1}^{M^\phi} C^{N,\phi,m}\beta_{Mm}(\mu) \right) \right\} \xi_{n,N,Mj}(\mu) = \lambda_{n,N,M}(\mu) \sum_{j=1}^{N} M_{i,j}^N \xi_{n,N,Mj}(\mu), \quad 1 \le i \le N, \quad 1 \le n \le n_e, \tag{41}$$

$$\sum_{i=1}^{N}\sum_{j=1}^{N} \xi_{n,N,Mi}(\mu) M_{i,j}^N \xi_{m,N,Mj}(\mu) = \delta_{nm}, \quad 1 \le n,m \le n_e, \tag{42}$$

where $A^N \in \mathbb{R}^{N\times N}$, $M^N \in \mathbb{R}^{N\times N}$, $C^{N,\phi,m} \in \mathbb{R}^{N\times N}$, $1 \le m \le M^\phi$ are given by $A_{i,j}^N = \tilde{a}_1(\zeta_j, \zeta_i; m_2^*) + \tilde{a}_2(\zeta_j, \zeta_i; V_b)$, $M_{i,j}^N = \tilde{a}_3(\zeta_j, \zeta_i)$, and $C_{i,j}^{N,\phi,m} = \tilde{a}_2(\zeta_j, \zeta_i; q_m^\phi)$ for $1 \le i,j \le N$.

Similarly, for Eqs. (34) and (35), we expand

$$d\xi_{n,N,M}(\mu) = \sum_{j=1}^{N} d\xi_{n,N,Mj}(\mu)\zeta_j, \tag{43}$$

where $\zeta_j \in W_N$, and $d\xi_{n,N,Mj}(\mu) \in \mathbb{R}$, and

$$d\phi_M(\cdot;\mu) = \sum_{m=1}^{M^{d\phi}} \gamma_{M,m}(\mu) q_m^{d\phi}(\cdot), \tag{44}$$

where $\gamma_M(\mu) \in \mathbb{R}^{M^{d\phi}}$ is given by

$$\sum_{k=1}^{M^{d\phi}} B^{M,d\phi}_{m,k}\gamma_{Mk}(\mu) = d\phi(t^{d\phi}_m;\mu), \quad 1 \le m \le M^{d\phi}, \quad (45)$$

and $B^{M,d\phi} \in \mathbb{R}^{M^{d\phi}} \times \mathbb{R}^{M^{d\phi}}$ is given by $B^{M,d\phi}_{m,k} = q^{d\phi}_m(t^{d\phi}_k)$, $1 \le m,k \le M^{d\phi}$. Inserting the above representations Eqs. (38), (43), and (44) into Eqs. (34) and (35), we obtain the following discrete equations:

$$\sum_{j=1}^{N} \left\{ A^N_{i,j} + \left(\sum_{m=1}^{M^\phi} C^{N,\phi,m}\beta_{Mm}(\mu) \right) - \lambda_{n,N,M}(\mu) M^N_{i,j} \right\} d\xi_{n,N,Mj}(\mu) = \sum_{j=1}^{N} \left\{ \frac{d\lambda_{i,N,M}(\mu)}{d\mu} M^N_{i,j} - \left(\sum_{m=1}^{M^{d\phi}} C^{N,d\phi,m}\gamma_{Mm}(\mu) \right) \right\} \xi_{n,N,Mj}(\mu), \quad 1 \le i \le N, \quad (46)$$

$$\sum_{i=1}^{N}\sum_{j=1}^{N} d\xi_{n,N,Mi}(\mu) M^N_{i,j} \xi_{n,N,Mj}(\mu) = 0, \quad (47)$$

where $C^{N,d\phi,m} \in \mathbb{R}^{N\times N}$, $1 \le m \le M^{d\phi}$ is given by $C^{N,d\phi,m}_{i,j} = \tilde{a}_2(\zeta_j,\zeta_i;q^{d\phi}_m)$, $1 \le i,j \le N$.

Finally, the linear functional $\tilde{a}_3$ is simply approximated by

$$\tilde{a}_3(w_n(\mu),v_m(\mu)) \approx \tilde{a}_3(w_{n,N,M}(\mu),v_{m,N,M}(\mu)) = \sum_{i=1}^{N}\sum_{j=1}^{N} M^N_{i,j} w_{n,N,Mi}(\mu) v_{m,N,Mj}(\mu). \quad (48)$$

The computational decomposition is then clear. At the beginning of each inner iteration, we generate nested reduced basis spaces W_N, $1 \le N \le N_{\max}$, nested approximation spaces W^ϕ_M, $1 \le M \le M^\phi_{\max}$ and $W^{d\phi}_M$, $1 \le M \le M^{d\phi}_{\max}$, and the associated nested sets of interpolation points T^ϕ_M and $T^{d\phi}_M$. For determining $\xi_{i,N,M}$, $1 \le i \le n_e$, we form and store $A^N, M^N, B^{M,\phi}$, $C^{N,\phi,m}$, $1 \le m \le M^\phi_{\max}$ and $C^{N,d\phi,m}$, $1 \le m \le M^{d\phi}_{\max}$. This is equivalent to the offline stage in a more typical reduced basis formulation. The computational cost is (to leading order) $O(N\mathcal{N}^\bullet + n_e N\mathcal{N}^\dagger + M^2N^2\mathcal{N})$, where $\bullet$ and $\dagger$ depend on the complexity of the eigenvalue solver and linear solver used, $M = \max(M^\phi, M^{d\phi})$, and $\mathcal{N}$ is the dimension of our "truth" approximation.

In the online stage—during construction of discrete matrices for Eq. (25)—we solve Eqs. (41) and (42) for $\xi_{n,N,Mj}(\mu)$, $1 \le j \le N$, $1 \le n \le n_e$, and Eqs. (46) and (47) for $d\xi_{n,N,Mj}(\mu)$, $1 \le j \le N^{d\xi_n}$, $1 \le n \le n_e$. Finally, we evaluate Eq. (48) in order to determine the $\tilde{a}_3$ terms in Eq. (25). The computational cost for each μ is then $O((n_eN)^3 + n_eN^3 + MN^2)$, which is then independent of $\mathcal{N}$.

D. *a posteriori* error estimation

The *a posteriori* error estimation procedure plays an important role in reduced basis method. An inexpensive estimate of the approximation error allows us to decide whether a reduced basis solution is sufficiently accurate for the purpose at hand. In addition, in the adaptive greedy algorithm to be outlined in Sec. III E, the error estimator serves as an efficient guide in the construction of the reduced basis sample set. The derivation of the *a posteriori* error estimator follows.[29] For $i = 1,\ldots,n_e$, we define the residual as

$$R_i(v;\mu) = \tilde{a}(\xi_{i,N,M}(\mu),v;V_{\text{eff}}(\mu)) - \lambda_{i,N,M}(\mu)\tilde{a}_3(\xi_{i,N,M}(\mu),v), \quad (49)$$

for $\forall v \in Y$ where $\tilde{a}(w,v;V_{\text{eff}}(\mu)) = \tilde{a}_1(w,v) + \tilde{a}_2(w,v;V_{\text{eff}}(\mu))$. We also define a reconstructed error $\hat{e}_i$ in Y, such that

$$\hat{a}(\hat{e}_i,v) = R_i(v;\mu), \quad \forall v \in Y, \quad (50)$$

where

$$\hat{a}(w,v) = \tilde{a}_1(w,v;m^*_2) + \tilde{a}_2(w,v;V_b) + \left(\gamma + \max_{\mu\in\mathcal{D},x_2\in\Omega^2} \phi(x_2;\mu)\right)\tilde{a}_3(w,v), \quad (51)$$

$$\gamma = \left| \min_{\mu\in\mathcal{D},x_2\in\Omega^2} \phi(x_2;\mu) \right|, \quad (52)$$

$$\|R_i(\cdot;\mu)\| \equiv \sup_{v\in Y} \frac{R_i(v;\mu)}{\hat{a}(v,v)^{1/2}} = \hat{a}(\hat{e}_i,\hat{e}_i)^{1/2}, \quad (53)$$

and $\|\cdot\| = \hat{a}(\cdot,\cdot)^{1/2}$.

Proposition 1. *Assume our reduced basis approximation is convergent in the sense that*

$$\lambda_{i,N,M}(\mu) \to \lambda_i(\mu), \quad 1 \le i \le n_e, \quad as \quad N \to \infty. \quad (54)$$

Then, for large N and $i = 1,\ldots,n_e$,

$$\left| \frac{\lambda_{i,N,M}(\mu) - \lambda_i(\mu)}{\lambda_i(\mu) + \gamma} \right| \le \frac{\|R_i(\cdot;\mu)\|}{[\lambda_{i,N,M}(\mu) + \gamma]^{1/2}}, \quad (55)$$

In addition, for $\lambda_{i,N,M}(\mu)$ *of multiplicity one and associated* $u_{N,i}(\mu)$, *we have*

$$\|u_{i,N,M}(\mu) - u_i(\mu)\| \le \frac{\|R_i(\cdot;\mu)\|}{d_i}, \quad (56)$$

and

$$|\lambda_{i,N,M}(\mu) - \lambda_i(\mu)| \le \frac{\|R_i(\cdot;\mu)\|^2}{d_i^2}, \quad (57)$$

where $d_i = \min_{j\ne i} \left| \frac{\lambda_{j,N,M}(\mu) - \lambda_{i,N,M}(\mu)}{\lambda_{j,N,M}(\mu) + \gamma} \right|$.

Proof. The proof is given in Appendix B. □

We note that Eq. (57) will in general be a better bound due to the $\|R_i\|^2$ term. Numerical experiments also indicate this is so. We thus define our error estimators based on Eqs. (56) and (57):

$$\Delta^{\lambda}_{N,M}(\mu) = \max_{1\le i\le n_e} \frac{1}{d_i^2}\frac{\|R_i(\cdot;\mu)\|^2}{|\lambda_{i,N,M}(\mu)|}, \tag{58}$$

$$\Delta^{\xi}_{N,M}(\mu) = \max_{1\le i\le n_e} \frac{1}{d_i}\frac{\|R_i(\cdot;\mu)\|}{\|\xi_{i,N,M}(\mu)\|}. \tag{59}$$

We can construct efficient offline-online computational strategies for the evaluation of our error estimators [Eqs. (58) and (59)]. From Eq. (51) and our reduced basis approximation, we have

$$\begin{aligned}\hat{a}(\hat{e}_i,v) = {}& \tilde{a}_1(\xi_{i,N,M}(\mu),v;m_2^*) + \tilde{a}_2(\xi_{i,N,M}(\mu),v;V_b)\\ &+ \sum_{m=1}^{M^\phi} \beta_m(\mu)\tilde{a}_2(\xi_{i,N,M}(\mu),v;q_m^\phi)\\ &+ \bar{\varepsilon}^\phi_{M+1}\tilde{a}_2(\xi_{i,N,M},v;q^\phi_{M^\phi+1})\\ &- \lambda_{i,N,M}(\mu)\tilde{a}_3(\xi_{i,N,M}(\mu),v), \quad v\in Y, \quad 1\le i\le n_e,\end{aligned} \tag{60}$$

where $\bar{\varepsilon}^\phi_M = \max_{\mu\in\mathcal{D}} \hat{\varepsilon}^\phi_M(\mu)$ and $\hat{\varepsilon}^\phi_M(\mu) = |\phi(t^\phi_{M^\phi+1};\mu) - \phi_M(t^\phi_{M^\phi+1};\mu)|$. It then follows from linear superposition that

$$\begin{aligned}\hat{e}_i(\mu) = {}& \sum_{n=1}^{N}\xi_{i,N,Mn}(\mu)\left\{p_n^1 + p_n^2 + \sum_{m=1}^{M^\phi}\beta_m p_n^{2+m} + \bar{\varepsilon}^\phi_M p_n^{M^\phi+3}\right\}\\ &- \lambda_{i,N,M}(\mu)\sum_{n=1}^{N}\xi_{i,N,Mn}(\mu)p_n^0,\end{aligned} \tag{61}$$

where

$$\hat{a}(p_n^1,v) = a_1(\zeta_n,v;m_2^*), \quad v\in Y, \quad 1\le n\le N,$$

$$\hat{a}(p_n^2,v) = a_2(\zeta_n,v;V_b), \quad v\in Y, \quad 1\le n\le N,$$

$$\hat{a}(p_n^{2+m},v) = a_2(\zeta_n,v;q_m^\phi), \quad v\in Y,$$

$$1\le n\le N, \quad 1\le m\le M^\phi+1,$$

$$\hat{a}(p_n^0,v) = a_3(\zeta_n,v), \quad v\in Y, \quad 1\le n\le N.$$

Then, $\|R_i(\cdot;\mu)\|$ is given by

$$\begin{aligned}\|R_i(\cdot;\mu)\|^2 = \hat{a}(\hat{e}_i,\hat{e}_i) = {}& \sum_{k=1}^{3+M^\phi}\sum_{k'=0}^{3+M^\phi}\sum_{n=1}^{N}\sum_{n'=1}^{N}\Theta_k(\mu)\Theta_{k'}(\mu)\xi_{i,N,Mn}(\mu)\xi_{i,N,Mn'}(\mu)\hat{A}^{k,k'}_{n,n'} + \sum_{n=1}^{N}\sum_{n'=1}^{N}\lambda^2_{i,N,M}(\mu)\xi_{i,N,Mn}(\mu)u_{i,N,Mn'}(\mu)\hat{A}^{0,0}_{n,n'}\\ &+ \sum_{n=1}^{N}\sum_{n'=1}^{N}\sum_{k=1}^{3+M^\phi}u_{N,in}(\mu)\lambda_{N,i}(\mu)\Theta_k(\mu)\hat{A}^{q,0}_{n,n'},\end{aligned} \tag{62}$$

where $\hat{A}^{k,k'}\in\mathbb{R}^{N\times N}$ are given by $\hat{A}^{k,k'}_{n,n'} = \hat{a}(p_n^k,p_{n'}^{k'})$, $0\le k,k'\le M^\phi+3$, $1\le n,n'\le N$, $\Theta_1=\Theta_2=1$, $\Theta_{2+m}=\beta_m$, $1\le m\le M^\phi$, and $\Theta_{M^\phi+3}=\bar{\varepsilon}^\phi_M$. We now see that the dual norm of the residual is the sum of products of parameter-dependent functions and parameter-independent functionals. The offline-online decomposition is now clear.

In the offline stage, we compute p_n^k, $0\le k\le M^\phi+3$, $1\le n\le N$, based on Eq. (60) at the cost of $O((4+M^\phi)N\mathcal{N}^\bullet)$, where the $\bullet$ denotes computational complexity of the linear solver used to obtain p_n^k. We then evaluate $\hat{A}^{k,k'}$ at the cost of $O((4+M^\phi)N^2\mathcal{N}^2)$. We store the matrices $\hat{A}^{k,k'}$ at a total cost of $(4+M^\phi)N^2$. In the online stage, we simply evaluate the sum [Eq. (61) for a given $\xi_{i,N,M}(\mu)$ and $\lambda_{i,N,M}(\mu)$, $1\le i\le n_e$. The operation count is only $O(n_e(M^\phi)^2N^2)$. The online complexity is thus independent of $\mathcal{N}$. Unless M^ϕ is large, the online cost to compute the error estimator is then a fraction of the cost required to obtain $\xi_{i,N,M}(\mu)$ and $\lambda_{i,N,M}(\mu)$.

E. Construction of reduced basis spaces

We now have all the components necessary to describe the greedy adaptive sampling procedure used to construct the sample sets S_N. A well-defined sample set is important as it will result in a rapidly convergent reduced basis approximation, and a well-conditioned reduced basis discrete system.

We first assume that we are given a sample S_N and hence a reduced basis space W_N, and the associated reduced basis approximation (procedure to determine) $\xi_{i,N,M}(\mu)$ and $\lambda_{i,N,M}(\mu)$, $\forall\,\mu\in\mathcal{D}$. We remind that $N=N_s n_e$. Then, for a suitably fine grid Ξ_μ over the parameter space $\mathcal{D}$, we determine $\mu^*_{N_s+1} = \arg\max_{\mu\in\Xi_\mu}\Delta^\lambda_{N,M}(\mu)$. Then we append $\mu^*_{N_s+1}$ to S_N to form S_{N+n_e} and hence W_{N+n_e}. The procedure is repeated until $\varepsilon_{\max} = \Delta^\lambda_{N,M}(\mu^*_{N_s+1})$ is below ε_{tol}, a tolerance we desire. This tolerance ε_{tol} determines the size of $N_{\max}$. Of course, we could use some other error measures instead of $\Delta^\lambda_{N,M}(\mu)$ defined in Eq. (58). However, the use of *a posteriori* error estimators as described in Sec. III D avoids determination of truth solution for all $\mu\in\Xi_\mu$, resulting in an efficient procedure. Due to its adaptive nature, this sampling procedure is relatively insensitive to the starting sample set, especially when the starting sample set S_{n_e} consists of only a single μ point. If we start with a poor μ point, the algorithm will next choose a good sample point based on our sampling criteria. This implies the effect of a poor starting μ point amounts to increasing N_s by 1.

F. Summary

The steps needed to implement the reduced basis method can be summarized as follows: (1) Construct approximation spaces W_M^{ϕ} and $W_M^{d\phi}$ for ϕ and $d\phi$ based on empirical interpolation approximation procedure. (2) Construct reduced basis approximation spaces W_N for ξ_i based on the adaptive greedy sampling procedure as described in Sec. III E. We need to construct two separate spaces (and approximations) for $m_2^*=m_t$ and $m_2^*=m_l$. During this step, we will have also constructed the relevant matrices needed to determine $\xi_{i,N,M}(\mu)$ and $d\xi_{i,N,M}(\mu)$, $1\le i\le n_e$ as described in Sec. III C, and $\Delta_{N,M}^{\lambda}(\mu)$, as described in Sec. III D. (3) Given a set of μ, we determine $\xi_{i,N,M}(\mu)$, $1\le i\le n_e$ from Eqs. (41) and (42) and $d\xi_{i,N,M}(\mu)$ from Eqs. (46) and (47). We can determine the error estimators $\Delta_{N,M}^{\lambda}(\mu)$ and $\Delta_{N,M}^{\xi}(\mu)$ based on Eqs. (58), (59), and (62).

We can now combine the reduced basis method and the subband decomposition method. Within each fixed-point iteration, part (i) of the solution method described in Sec. II B will now consist of (a) offline stage—steps 1 and 2—in which we construct the reduced basis machinery required to approximate $\xi_i(x_2;x_1)$ and $\lambda_i(x_1)$, and their derivatives to a required level of accuracy, and (b) online stage—step 3—in which we approximate $\xi_i(x_2;x_1)$ and $\lambda_i(x_1)$ for finite points on Ω_1 by $\xi_{i,N,M}(x_2;x_1)$ and $\lambda_{i,N,M}(x_1)$. Note that steps 1 and 2 are computationally intensive and we would like to avoid implementing the offline stage at each fixed-point iteration. This is indeed possible. Armed with the *a posteriori* error estimators, we only need to reconstruct the reduced basis machinery when the estimated errors of the solutions based on W_N of the previous iteration are above the tolerance we desired. This significantly reduces the cost of reduced basis method by limiting the number of times we need to perform the expensive offline computation. The procedure is summarized in Fig. 3.

There are several variations to the above procedure. For example, a more frequent reconstruction may lead to smaller N, thus reducing the cost of "online" calculation. Thus, one could impose compulsory reconstruction of W_N at fixed intervals; at present we do not impose this as N required is generally small. In addition, we do not expect N to change drastically since ϕ only changes slightly between iterations. We could also reduce the offline computational cost by reconstructing the W_N based on existing S_N. While this removes the cost associated with greedy sampling procedure, we are less certain that the approximation space will be optimal and the solutions within the tolerance we desired.

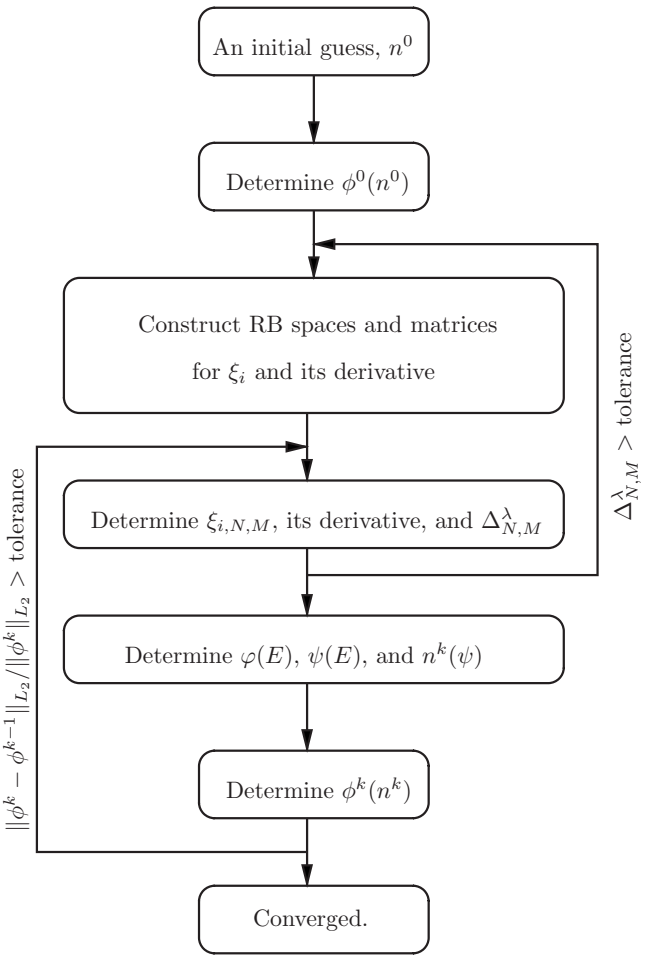

FIG. 3. Subband decomposition procedure with reduced basis approximation in part (i).

IV. NUMERICAL RESULTS

We consider a domain $\Omega=[0,580]\times[0,100]$, which is divided into five subdomains detailed in Table I. The relative dielectric constant, ϵ_r, and donor concentration, N_D, in each subdomain are also listed in Table I. The source voltage V_S and the gate voltage V_G are maintained at 0 and 0.015, respectively; the drain voltage V_D is allowed to vary between 0 and 0.015, and the applied temperature is 9.5×10^{-4} (approximately 300 K). We assume $n_e=8$ gives a sufficiently accurate approximation. To evaluate Eq. (20), we use $E_{\max}=20$ T (since $f_{1/2}(-E_{\max}/T)<10^{-8}$), $n_{\mathbf{k}}=120$ and $Q=3$.

We will first look at the convergence properties of the empirical interpolation approximation for ϕ and $\partial\phi/\partial x_1$ and the reduced basis approximation for $\xi_i(x_1)$, $1\le i\le n_e$. We then compare effects of using reduced basis method in part (i) on accuracy and efficiency of subband decomposition method. In our fixed-point iterative scheme, the convergence criteria are given by $\|\phi^k-\phi^{k-1}\|_{L_2}/\|\phi^k\|_{L_2}<10^{-4}$. All results are for a discretization where the grid size in the x_1 direction, h_1, is 5 and the grid size in the x_2 direction, h_2, is 2.

TABLE I. Definition of $\Omega_1-\Omega_5$, and ϵ_r and N_D used in the model problem; $\epsilon_0=1/4\pi$.

	Extent	$\epsilon_r=\epsilon/\epsilon_0$	N_D
Ω_1	$[200,380]\times[20,80]$	11.7	0
Ω_2	$[0,200]\times[20,80]$	11.7	2.96×10^{-5}
Ω_3	$[380,580]\times[20,80]$	11.7	2.96×10^{-5}
Ω_4	$[0,580]\times[80,100]$	3.9	0
Ω_5	$[0,580]\times[0,20]$	3.9	0

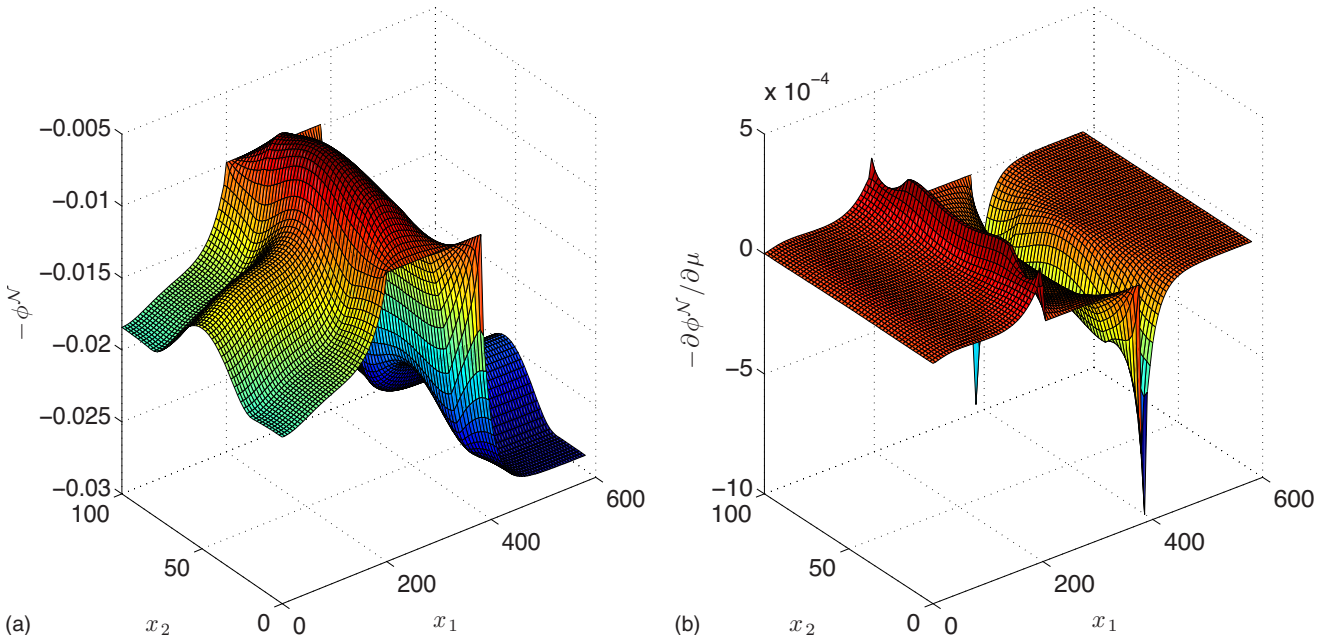

FIG. 4. (Color online) $\phi^{\mathcal{N}}$(left) and $\partial\phi^{\mathcal{N}}/\partial\mu$ (right) for V_D=0.015. The superscript $\mathcal{N}$ indicates that it is a finite element approximation of ϕ.

A. Empirical interpolation approximation of ϕ and $\partial\phi/\partial\mu$

We first examine the approximation of ϕ and $\partial\phi/\partial\mu$ based on the empirical interpolation method. Figure 4 shows the solutions of ϕ and $\partial\phi/\partial\mu$ at convergence for the case V_D=0.015. We note that the variation of $\phi(x_2;\mu)$ with respect to μ is nontrivial. The empirical interpolation errors of ϕ_M and $\partial\phi_M/\partial\mu$, denoted by $\bar{\varepsilon}_M^{\phi}$ and $\bar{\varepsilon}_M^{d\phi}$, respectively, are shown in Fig. 5. The figure shows that we have a rapidly converging approximation—with M^{ϕ}=21 and $M^{d\phi}$=23, the errors $\bar{\varepsilon}_M^{\phi}$ and $\bar{\varepsilon}_M^{d\phi}$ are less than 10^{-8}.

B. Convergence of the reduced basis approximation

For our convergence analysis, the test sample Ξ_μ is given by the number of grid points in the x_1 direction—for the current discretization, the size of Ξ_μ is 117. We define the following error measures:

$$\varepsilon_{N,M}^{\lambda} = \max_{\mu\in\Xi_\mu} \epsilon_{N,M}^{\lambda}(\mu), \quad \varepsilon_{N,M}^{\xi} = \max_{\mu\in\Xi_\mu} \epsilon_{N,M}^{\xi}(\mu), \tag{63}$$

where

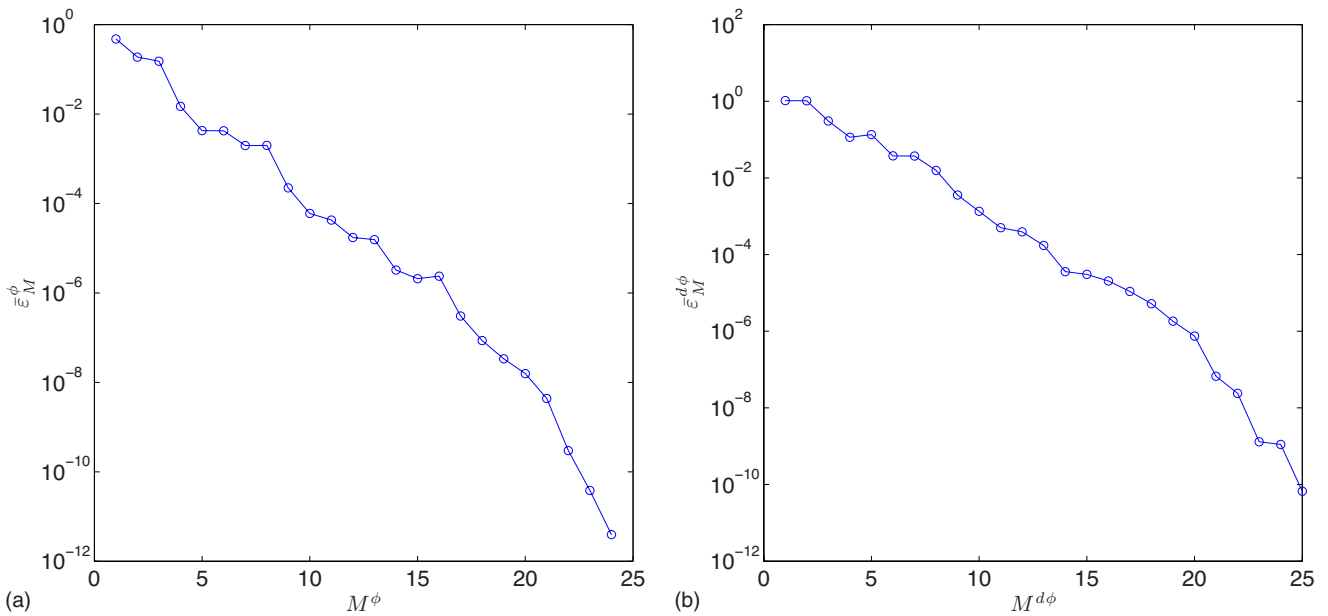

FIG. 5. (Color online) ε_M versus M for ϕ_M (left) and $\frac{\partial\phi_M}{\partial\mu}$ (right).

TABLE II. Convergence of the reduced basis approximation for $V_D=0.015$.

N_s	N	$\varepsilon^{\lambda}_{N,M}$	$\varepsilon^{\xi}_{N,M}$	$\max_{\mu\in\Xi_\mu} \Delta^{\lambda}_{N,M}$	$\max_{\mu\in\Xi_\mu} \Delta^{\xi}_{N,M}$	$\max_{\mu\in\Xi_\mu} \eta^{\lambda}_{N,M}$	$\max_{\mu\in\Xi_\mu} \eta^{\xi}_{N,M}$
				$m_2^*=m_l$			
1	8	6.12E-4	3.28E-2	4.70E-3	5.18E-2	1.03E+2	6.15E+0
2	16	4.60E-6	3.50E-4	6.30E-5	1.17E-3	4.93E+1	6.60E+0
1	24	2.01E-10	1.10E-5	3.17E-9	4.15E-5	4.26E+1	4.14E+1
				$m_2^*=m_t$			
1	8	4.15E-4	3.35E-2	6.22E-3	7.10E-2	4.56E+1	5.39E+0
2	16	5.76E-7	8.45E-4	2.40E-5	4.53E-3	6.48E+1	7.49E+0
3	24	1.87E-10	1.29E-5	6.95E-9	7.39E-5	5.84E+1	7.40E+0

$$\epsilon^{\lambda}_{N,M}(\mu) = \max_{1\le i\le n_e} \frac{|\lambda_{i,N,M}(\mu)-\lambda_i(\mu)|}{|\lambda_i(\mu)|}, \tag{64}$$

$$\epsilon^{\xi}_{N}(\mu) = \max_{1\le i\le n_e} \frac{\|\xi_{i,N,M}(\mu)-\xi_i(\mu)\|}{\|\xi_i(\mu)\|}. \tag{65}$$

We also define the effectivity measures as

$$\eta^{\lambda}_{N,M}(\mu) = \frac{\Delta^{\lambda}_{N,M}(\mu)}{\epsilon^{\lambda}_{N,M}(\mu)}, \quad \eta^{\xi}_{N,M}(\mu) = \frac{\Delta^{\xi}_{N,M}(\mu)}{\epsilon^{\xi}_{N,M}(\mu)}. \tag{66}$$

Table II shows that our reduced basis approximation is rapidly convergent. For both $m_2^*=m_l$ and m_t, we require only 24 basis functions to reduce the relative errors $\varepsilon^{\lambda}_{N,M}$ to below 10^{-8} and $\varepsilon^{\xi}_{N,M}$ to below 10^{-4} for the case where $V_D=0.015$. In addition, the effectivity measures are small, indicating that our error estimators are good surrogates to the actual errors. Although $\eta^{\lambda}_{N,M}$ and $\eta^{\xi}_{N,M}$ increase with N, $\Delta^{\lambda}_{N,M}$ and $\Delta^{\xi}_{N,M}$ also decrease—thus the absolute difference between the actual errors and the error estimators is small.

We now look at the reduced basis errors in $d\xi_{i,N,M}(\cdot)$, $d\lambda_{i,N,M}(\cdot)$, $1\le i\le n_e$ and $\tilde{a}_3(d\xi_{i,N,M},\xi_{j,N,M})$, $1\le i,j,\le n_e$. We define

$$\varepsilon^{d\lambda}_{N,M} = \max_{\mu\in\Xi_\mu} \max_{1\le i\le n_e} \frac{|d\lambda_{i,N,M}(\mu)-d\lambda_i(\mu)|}{|d\lambda_i(\mu)|}, \tag{67}$$

$$\varepsilon^{d\xi}_{N,M} = \max_{\mu\in\Xi_\mu} \max_{1\le i\le n_e} \frac{\|d\xi_{i,N,M}(\mu)-d\xi_i(\mu)\|}{\|d\xi_i(\mu)\|}, \tag{68}$$

$$\varepsilon^{\tilde{a}_3}_{N,M} = \max_{\mu\in\Xi_\mu} \max_{1\le i,j\le n_e} \times \frac{|\tilde{a}_3(d\xi_{i,N,M}(\mu),\xi_{j,N,M}(\mu))-\tilde{a}_3(d\xi_i(\mu),\xi_j(\mu))|}{|\tilde{a}_3(d\xi_i(\mu),\xi_j(\mu))|}. \tag{69}$$

From Table III, we again see the rapid convergence in the errors defined by Eqs. (67)–(69). In particular, the error in $\tilde{a}_3(\cdot,\cdot)$, which determines the effects of reduced basis approximation on the subband decomposition method, decreases rapidly with N. For a relative error of 10^{-5}, $N=24$ is sufficient for both $m_2^*=m_l$ and m_t. Since the magnitude of $\tilde{a}_3(d\xi_i(\mu),\xi_j(\mu))$ is of order 10^{-4}, the absolute error in the approximation is actually very small.

As mentioned in Sec. III B, we now examine the approximation of $d\xi_i(\mu)$ in W_N^d given by Eq. (37). We note that the solutions $(\xi_{i,N,M},\lambda_{i,N,M})$ must also be determined in $W_N^d\times\mathbb{R}$. From Table IV, we indeed see a faster convergence in the errors with respect to N_s. However, the total number of basis, N, also increases with N_s at a rate double that of W_N. As such, for higher accuracy, W_N^d can indeed be a better approximation space although for the current purpose, W_N appears to be sufficient and leads to a smaller N.

C. Effects of reduced basis approach on efficiency of subband decomposition method

We denote the methods where we approximate part (i) of the subband decomposition method by finite element method and reduced basis method as SDM/FEM and SDM/RBM, respectively; parts (ii) and (iii) are approximated by finite element method for both approaches. The finite element approximation of part (i) is implemented using $\mathbb{P}_1$ elements with $\mathcal{N}=51$ while the reduced basis approximation uses the accuracy criteria given by $\Delta^{\lambda}_{N,M}<10^{-7}$. To compare the accuracies of the two approaches, we compare the solutions

TABLE III. Convergence of the reduced basis approximation of $d\lambda_{i,N,M}$ and $d\xi_{i,N,M}$, $1\le i\le n_e$ for $V_D=0.015$.

N_s	N	$\varepsilon^{d\lambda}_{N,M}$	$\varepsilon^{d\xi}_{N,M}$	$\varepsilon^{\tilde{a}_3}_{N,M}$
		$m_2^*=m_l$		
1	8	3.6911E-2	9.4697E-1	6.8170E+0
2	16	1.9097E-5	7.4886E-2	1.4036E-2
3	24	9.4836E-8	1.6339E-3	8.8105E-6
		$m_2^*=m_t$		
1	8	4.2302E-2	8.4431E-1	4.0849E+0
3	16	5.2726E-4	2.2922E-1	1.2190E-2
3	24	4.1623E-8	3.0825E-3	5.6612E-6

TABLE IV. Convergence of the reduced basis approximation of $d\lambda_{i,N,M}$ and $d\xi_{i,N,M}$, $1 \le i \le n_e$ for $V_D=0.015$ with W_N^d. The results are for $m_2^*=m_l$.

N_s	N	$\varepsilon_{N,M}^{d\lambda}$	$\varepsilon_{N,M}^{d\xi}$	$\varepsilon_{N,M}^{\tilde{a}_3}$
1	16	4.5909E-4	4.2958E-2	3.0776E-3
2	32	3.1253E-11	4.9611E-6	9.4168E-9

obtained to a full finite element implementation; i.e., Eq. (15) is directly approximated by a finite element method utilizing $\mathbb{Q}_2$ elements. We denote the density obtained with this full finite element implementation by n_t.

From Table V, we first note that the accuracies in $\phi^{\mathcal{N}}$ obtained by the two approaches are comparable—the relative errors of $\phi^{\mathcal{N}}(n^{\mathcal{N}})$ and $\phi^{\mathcal{N}}(n_{N,M})$ to $\phi^{\mathcal{N}}(n_t)$ are of the same order of magnitude. Here, $n^{\mathcal{N}}$ and $n_{N,M}$ are respectively the densities computed based on the SDM/FEM and SDM/RBM approaches. This implies that part (i) can be approximated by the reduced basis method without any adverse effect on the accuracy level of the subband decomposition method. More remarkably, this is achieved with a factor-of-5 reduction in the computational time spent in part (i), which includes the cost of constructing the relevant matrices for use in part (ii). We further note that the reduced basis approximation spaces are only reconstructed once and twice for the whole duration of the simulation.

However, due to the computational overhead in parts (ii) and (iii), the total computational savings achieved with the SDM/RBM approach are more modest for the discretization we have used—the reduction in the computational time is less than a factor of 2. Part (iii) is particularly computationally intensive as it involves solving a nonlinear PDE in a two-dimensional domain. Nevertheless, we expect the reduction in total computational time to increase as we refine the resolution in the x_2 direction. Figure 6 shows how the total computational time and computational time spent in part (i) scale with respect to h_2 where h_2 is the mesh spacing in the x_2 direction; the reported time has been scaled with respect to the total computational time of SDM/RBM at $h_2=4$. With the SDM/FEM approach, the computational time spent in part (i) increases rapidly as h_2 decreases while with the SDM/RBM approach, we only see a marginal increase in the computational time. This marginal increase is due to the slight increase in the computational cost of the offline stage; there should be little or no increase in the computational cost of the online stage. On the other hand, when we compare the total computational time of the two approaches, the gain in the computational savings as h_2 decreases is less impressive. We achieve a factor of 2 when $h_2=0.5$. This is because as h_2 decreases, the dimension of the nonlinear Poisson equation we are solving in part (iii) also increases, leading to a rapid increase in the computational cost of part (iii). We note that the computational time of part (ii) should remain unchanged, as long as h_1 remains the same. The above observation strongly suggests that the reduced basis approach is particularly suited for situations where computational cost of part (i) dominates the total computational cost. For example, fine resolution may be needed in the x_2 direction due to strong confinement of the electrons. In nanowires and nanotubes where we have a two-dimensional confinement, the higher dimension will also lead to larger mesh size, thus increasing the computational cost of part (i).

Finally, we look at a how the drain current per unit width I_D varies with drain voltage V_D. Figure 7 shows that we have a typical current-voltage relation for a MOSFET, where the rate of increase in I_D decreases as the applied voltage V_D increases. We further note that the SDM/RBM method gives a comparable result to the SDM/FEM method.

V. CONCLUSION

We have described how reduced basis method can improve the efficiency of the subband decomposition approach to ballistic transport simulation in nanodevices. In particular, the use of *a posteriori* error estimator and adaptive sampling procedure leads to a very efficient solution procedure. Numerical results based on a double-gate MOSFET show that the computational cost is reduced by 50% for a reasonably sized problem and depends very weakly on the mesh size in the confined direction. We expect the computational savings to increase in cases of 2D confinement, such as those encountered in nanowires.

ACKNOWLEDGMENTS

I would like to thank A. T. Patera, Y. Maday and C. Le Bris for their guidance, and J. B. Bell for useful discussions. This work was supported by the Director, Office of Science,

TABLE V. Comparison of the computational cost for the subband decomposition method and the reduced basis method. Here N_{offline} is the number of times W_N is reconstructed; $k_{\max}$ is the maximum number of fixed-point iteration; $n^{\mathcal{N}}$ is obtained from the SDM/FEM approach; $n_{N,M}$ is obtained from the SDM/RBM approach; and n_t is obtained from a full finite element approximation.

	SDM/FEM			SDM/RBM				
	Time, s			Time, s				
Case	Total	part (i)	$\frac{\|\phi^{\mathcal{N}}(n^{\mathcal{N}})-\phi^{\mathcal{N}}(n_t)\|_{L_2}}{\|\phi^{\mathcal{N}}(n_t)\|_{L_2}}$	Total	part (i)	$\frac{\|\phi^{\mathcal{N}}(n_{N,M})-\phi^{\mathcal{N}}(n_t)\|_{L_2}}{\|\phi^{\mathcal{N}}(n_t)\|_{L_2}}$	N_{offline}	$k_{\max}$
$V_D=0$	495	239	7.74E-4	302	45	8.19E-4	2	10
$V_D=0.015$	417	216	8.48E-4	246	41	8.33E-4	1	9

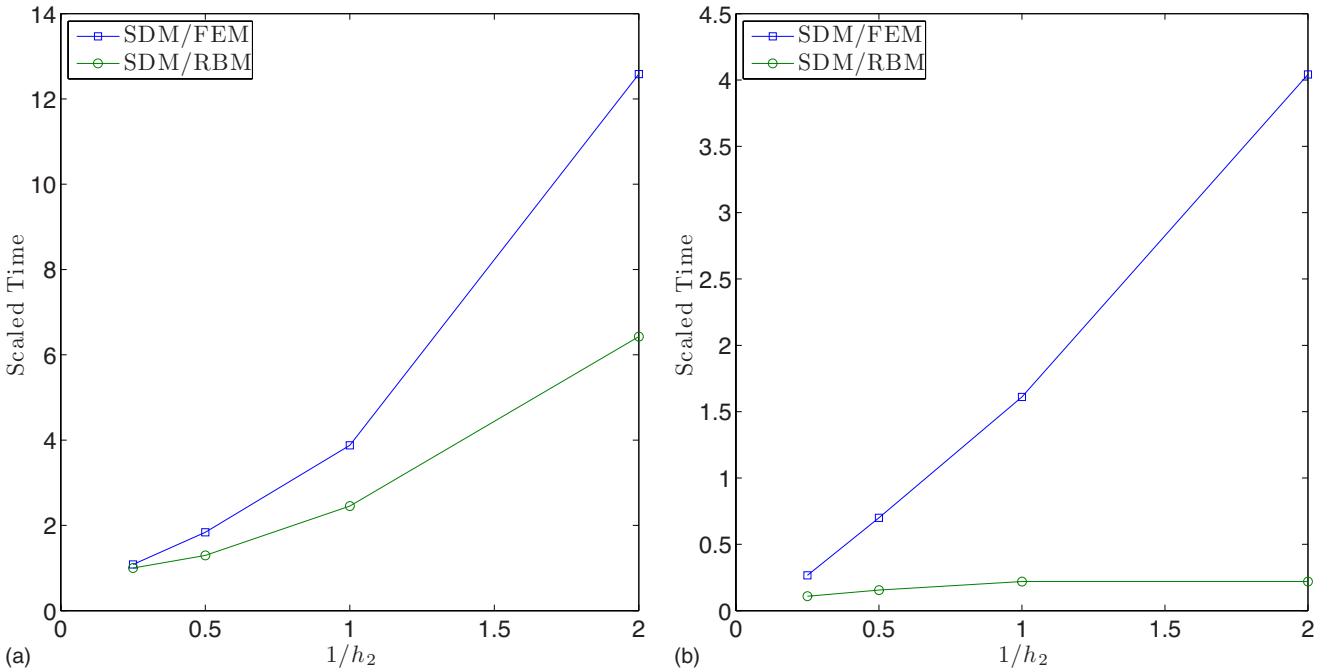

FIG. 6. (Color online) Comparison of (a) the total computational time and (b) the computational time for part (i), for the subband decomposition method and the reduced basis method with increasing mesh size. The time is scaled with respect to total time for the SDM/RBM method at $h_2=4$.

of the U.S. Department of Energy under Contract No. DE-AC02-05CH11231.

APPENDIX A: ATOMIC UNITS

Atomic units are used throughout this paper. Table VI lists the conversion between atomic units and common units of some relevant quantities.

APPENDIX B: PROOF OF PROPOSITION 1

We first note that the eigenvalues λ_i are of multiplicity *one* but $\tilde{a}(v,v;V_{\text{eff}}(\mu))=\tilde{a}_1(v,v;m_2^*)+\tilde{a}_2(v,v;V_{\text{eff}}(\mu))$ is not strictly positive for all $\mu\in\mathcal{D}$. To derive the bounds given by Eqs. (55)–(57), we need to first define a surrogate functional form that will be positive for all $\mu\in\mathcal{D}$. For this purpose, we define $\tilde{a}^+(w,v;V_{\text{eff}}(\mu))=\tilde{a}(w,v;V_{\text{eff}}(\mu))+\gamma\tilde{a}_3(w,v)$ and introduce the following eigenvalue problem: for $\mu\in\mathcal{D}$, find $(\xi_i^+(\mu),\lambda_i^+(\mu))\in Y\times\mathbb{R}$, $1\le i\le n_e$ such that

$$\tilde{a}^+(\xi_i^+(\mu),v;V_{\text{eff}}(\mu))=\lambda_i^+(\mu)\tilde{a}_3(\xi_i^+(\mu),v), \qquad \text{(B1)}$$

$$\forall v\in Y,\quad 1\le i\le n_e,$$

$$\tilde{a}_3(\xi_i^+(\mu),\xi_j^+(\mu))=\delta_{ij},\quad 1\le i\le j\le n_b. \qquad \text{(B2)}$$

It is clear that $\xi_i^+(\mu)=\xi_i(\mu)$ and $\lambda_i^+=\lambda_i+\gamma$.

Proposition 2. *Given* $\hat{a}(w,v)$ *as defined in* Eq. (51), *we have*

$$\hat{a}(v,v)\ge\tilde{a}^+(v,v;V_{\text{eff}}(\mu))\ge\tilde{a}_3(v,v)\ge 0, \qquad \text{(B3)}$$

for all $\mu\in\mathcal{D}$.

Proof. We first prove the left inequality. Let $f(\cdot)=\max_{\mu\in\mathcal{D},x_2\in\Omega^2}\phi(x_2;\mu)$. By expanding $\tilde{a}^+$, we obtain

$$\begin{aligned}\tilde{a}^+(v,v;V_{\text{eff}}(\mu))&=\tilde{a}_1(v,v;m_2^*)+\tilde{a}_2(v,v;V_b)+\tilde{a}_2(v,v;\phi(\mu))\\&\quad+\gamma\tilde{a}_3(v,v)\le\tilde{a}_1(v,v;m_2^*)+\tilde{a}_2(v,v;V_b)\\&\quad+\tilde{a}_2(v,v;f)+\gamma\tilde{a}_3(v,v),\end{aligned} \qquad \text{(B4)}$$

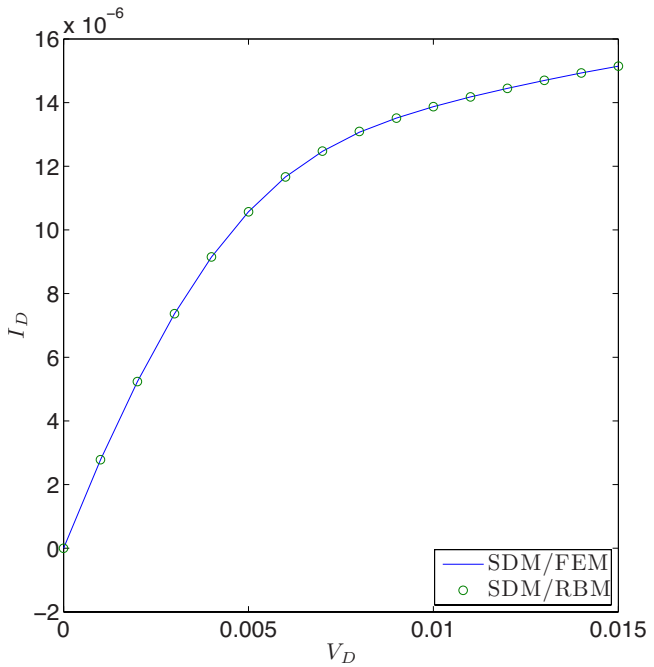

FIG. 7. (Color online) Comparison of the computed drain current for SDM/FEM and SDM/RBM.

TABLE VI. Conversion between atomic units of magnitude 1 to some other common units.

	Common units
Length	5.29177211×10^{-2} nm
Temperature	3.15774645×10^{5} K
Energy	27.21138386 eV
Electric potential	27.21138386 eV
Current per unit width	1.25168236×10^{8} A/m
Density of states	6.74833453×10^{30} m^{-3}

since $\tilde{a}_1(v,v;m_2^*)\geq 0$; $\tilde{a}_2(v,v;V_b)\geq 0$ as $V_b\geq 0$, $\tilde{a}_3(v,v)\geq 0$, and $\gamma\geq 0$. Since the right-hand side of Eq. (B4) is equivalent to $\hat{a}(v,v)$, the left inequality is proven.

To prove the right inequality, we first note that

$$\tilde{a}(v,v;V_{\text{eff}}(\mu))\geq \lambda_1(\mu)\tilde{a}_3(v,v),$$

and $\lambda_1(\mu)\geq \min_{x_2\in\Omega^2}\{V_b(x_2)+\phi(x_2;\mu)\}$. Then,

$$\begin{aligned}\tilde{a}^+(v,v;V_{\text{eff}}(\mu)) &= \tilde{a}(v,v;V_{\text{eff}}(\mu)) \\ &\quad + \left|\min_{\mu\in\mathcal{D},x_2\in\Omega_2}\phi(x_2;\mu)\right|\tilde{a}_3(v,v) \\ &\geq \left[\min_{\mu\in D}\lambda_1(\mu)+\left|\min_{\mu\in\mathcal{D},x_2\in\Omega_2}\phi(x_2;\mu)\right|\right]\tilde{a}_3(v,v) \\ &\geq \tilde{a}_3(v,v), \end{aligned} \tag{B5}$$

since $\min_{x_2\in\Omega^2} V_b(x_2)=0$ and $\min_{\mu\in D}\lambda_1(\mu)+\left|\min_{\mu\in\mathcal{D},x_2\in\Omega_2}\phi(x_2;\mu)\right|\geq 0$. This concludes the proof for Proposition 2.

Hypothesis 1. *Assuming our reduced basis approximation is convergent in the sense that*

$$\lambda_{i,N,M}(\mu)\to\lambda_i(\mu),\quad 1\leq i\leq n_e,\quad \text{as}\quad N\to\infty. \tag{B6}$$

Then, for sufficiently large N,

$$i=\arg\min_{1\leq j\leq\mathcal{N}}\left|\frac{\lambda_{i,N,M}(\mu)-\lambda_j(\mu)}{\lambda_j^+(\mu)}\right|. \tag{B7}$$

The proof of Proposition 1 then utilizes Proposition 2 and Hypothesis 1. The rest of the proof can be found in Ref. 29.

APPENDIX C: DERIVATIVE OF ϕ

To solve Eq. (25), we must evaluate $\partial\xi_n/\partial x_1$; in Ref. 10, ξ_n, $\partial\xi_n/\partial x_1$ and $\tilde{a}_3(\cdot,\cdot)$ are evaluated at the nodes (i,j) of the rectangular mesh, and interpolated to the quadrature points when evaluating the functionals in Eq. (25). In addition, $\partial\xi_n/\partial x_1$ are evaluated by a difference formula. In our approach, $\partial\xi_n/\partial x_1$ are determined from Eq. (27), and this involves determining $\partial\phi/\partial x_1$ at the nodes (i,j). However, as we have used $\mathbb{Q}_2$ elements to solve for ϕ, its derivative is discontinuous, and thus not defined at the nodes. So, we compute the $\partial\phi/\partial x_1$ based on a difference formula. We then compute ξ_n, $\partial\xi_n/\partial x_1$ and $\tilde{a}_3(\cdot,\cdot)$ at the nodes (i,j) of the rectangular mesh, and interpolate to the quadrature points when evaluating the functionals in Eq. (25).

To avoid evaluating $\partial\phi/\partial x_1$ at the nodes, we can choose to compute $\partial\xi_n/\partial x_1$ directly at the quadrature points used to evaluate the functionals in Eq. (25). The reduced basis approximation procedure is as follows: (1) Compute $\partial\phi/\partial x_1$ at $(i+1/2,j)$, where $i+1/2$ is the midpoint between i and $i+1$. (2) Construct a magic point approximation for $\partial\phi/\partial x_1$, and the reduced basis machinery for $\partial\xi_n/\partial x_1$. (3) Evaluate the terms $\xi_{n,N,M}$, $\partial\xi_{n,N,M}/\partial x_1$ and $\tilde{a}_3$ at the quadrature points. To evaluate $\xi_{n,N,M}$ and $\partial\xi_{n,N,M}/\partial x_1$, values of ϕ_M and $\partial\phi_M/\partial x_1$ at the magic points for a given quadrature point must first be determined. For ϕ_M, these are obtained by the interpolation of the $\mathbb{Q}_2$ elements. For $\partial\phi_M/\partial x_1$, since the gradient between node $(i,t_M^{d\phi})$ and $(i+1,t_M^{d\phi})$ is a constant, the values at the magic points for quadrature point falling between $(i,t_M^{d\phi})$ and $(i+1,t_M^{d\phi})$ is given by the value at node $(i+1/2,t_M^{d\phi})$; $t_M^{d\phi}$ are the magic points for $\partial\phi_M/\partial x_1$.

The above formulation should then be consistent with the $\mathbb{Q}_2$ elements we use. It is however more expensive: the computational cost of part (i) is increased by 66%. Determining the accuracy of the two approaches is also tricky. A comparison to, say, a full finite element approximation may be necessary although approximation error of subband decomposition method may dominate. In addition, the convergence criteria used in the fixed-point iteration are not stringent, and any difference between the two approaches may not be discernible.

*gpau@lbl.gov

[1] K. Natori, J. Appl. Phys. **76**, 4879 (1994).
[2] C. S. Lent and D. J. Kirkner, J. Appl. Phys. **67**, 6353 (1990).
[3] E. Polizzi and N. Ben Abdallah, Phys. Rev. B **66**, 245301 (2002).
[4] S. E. Laux, A. Kumar, and M. V. Fischetti, J. Appl. Phys. **95**, 5545 (2004).
[5] R. Venugopal, Z. Ren, S. Datta, M. S. Lundstrom, and D. Jovanovic, J. Appl. Phys. **92**, 3730 (2002).
[6] Z. Ren, R. Venugopal, S. Goasguen, S. Datta, and M. Lundstrom, IEEE Trans. Electron Devices **50**, 1914 (2003).
[7] A. Trellakis, A. T. Galick, A. Pacelli, and U. Ravaioli, J. Appl. Phys. **81**, 7880 (1997).
[8] L. R. Ram-Mohan, K. H. Yoo, and J. Moussa, J. Appl. Phys. **95**, 3081 (2004).
[9] L. R. Ram-Mohan, *Finite Element and Boundary Element Applications to Quantum Mechanics* (Oxford University, Oxford, 2002).
[10] E. Polizzi and N. B. Abdallah, J. Comput. Phys. **202**, 150 (2005).
[11] N. B. Abdallah, M. Mouis, and C. Negulescu, J. Comput. Phys. **225**, 74 (2007).
[12] J. Wang, E. Polizzi, and M. Lundstrom, J. Appl. Phys. **96**, 2192 (2004).

[13] B. O. Almroth, P. Stern, and F. A. Brogan, AIAA J. **16**, 525 (1978).
[14] A. K. Noor and J. M. Peters, AIAA J. **18**, 455 (1980).
[15] J. P. Fink and W. C. Rheinboldt, Z. Angew. Math. Mech. **63**, 21 (1983).
[16] M. D. Gunzburger, *Finite Element Methods for Viscous Incompressible Flows* (Academic, New York, 1989).
[17] K. Ito and S. S. Ravindran, J. Comput. Phys. **143**, 403 (1998).
[18] J. S. Peterson, SIAM (Soc. Ind. Appl. Math.) J. Sci. Stat. Comput. **10**, 777 (1989).
[19] T. A. Porsching, Math. Comput. **45**, 487 (1985).
[20] M. A. Grepl, N. C. Nguyen, K. Veroy, A. T. Patera, and G. R. Liu, in Proceedings of the Second Sandia Workshop of PDE-Constrained Optimization: Towards Real-Time PDE-Constrained Optimization, SIAM Computational Science and Engineering Book Series (SIAM, Philadelphia, 2007), pp. 197–215.
[21] L. Machiels, Y. Maday, I. B. Oliveira, A. Patera, and D. Rovas, C. R. Math. **331**, 153 (2000).
[22] Y. Maday, A. T. Patera, and G. Turinici, C. R. Math. **335**, 289 (2002).
[23] C. Prud'homme, D. Rovas, K. Veroy, Y. Maday, A. Patera, and G. Turinici, ASME J. Fluids Eng. **124**, 70 (2002).
[24] N. C. Nguyen, K. Veroy, and A. T. Patera, in *Handbook of Materials Modeling*, edited by S. Yip (Springer, New York, 2005), pp. 1523–1558.
[25] K. Veroy and A. T. Patera, Int. J. Numer. Methods Fluids **47**, 773 (2005).
[26] K. Veroy, C. Prud'homme, D. V. Rovas, and A. T. Patera, Proceedings of the 16th AIAA Computational Fluid Dynamics Conference, 2003, Paper No. 2003-3847.
[27] M. Barrault, N. C. Nguyen, Y. Maday, and A. T. Patera, C. R. Math. **339**, 667 (2004).
[28] M. A. Grepl, Y. Maday, N. C. Nguyen, and A. T. Patera, Math. Modell. Numer. Anal. **41**, 575 (2007).
[29] G. S. H. Pau, Phys. Rev. E **76**, 046704 (2007).
[30] G. Bastard, *Wave Mechanics Applied to Semiconductor Heterostructures* (Wiley, New York, 1991).
[31] Y. Maday, N. C. Nguyen, A. T. Patera, and G. S. Pau (unpublished).